Water Splitting Hot Paper

International Edition: DOI: 10.1002/anie.201916681
German Edition: DOI: 10.1002/ange.201916681

Activation of Water-Splitting Photocatalysts by Loading with Ultrafine Rh–Cr Mixed-Oxide Cocatalyst Nanoparticles

*Wataru Kurashige, Yutaro Mori, Shuhei Ozaki, Masanobu Kawachi, Sakiat Hossain, Tokuhisa Kawawaki, Cameron J. Shearer, Akihide Iwase, Gregory F. Metha, Seiji Yamazoe, Akihiko Kudo, and Yuichi Negishi**

Abstract: *The activity of many water-splitting photocatalysts could be improved by the use of Rh^{III}–Cr^{III} mixed oxide ($Rh_{2-x}Cr_xO_3$) particles as cocatalysts. Although further improvement of water-splitting activity could be achieved if the size of the $Rh_{2-x}Cr_xO_3$ particles was decreased further, it is difficult to load ultrafine (<2 nm) $Rh_{2-x}Cr_xO_3$ particles onto a photocatalyst by using conventional loading methods. In this study, a new loading method was successfully established and was used to load $Rh_{2-x}Cr_xO_3$ particles with a size of approximately 1.3 nm and a narrow size distribution onto a $BaLa_4Ti_4O_{15}$ photocatalyst. The obtained photocatalyst exhibited an apparent quantum yield of 16%, which is the highest achieved for $BaLa_4Ti_4O_{15}$ to date. Thus, the developed loading technique of $Rh_{2-x}Cr_xO_3$ particles is extremely effective at improving the activity of the water-splitting photocatalyst $BaLa_4Ti_4O_{15}$. This method is expected to be extended to other advanced water-splitting photocatalysts to achieve higher quantum yields.*

Introduction

With increasing the global warming and the depletion of fossil resources, society is expected to shift to using clean and renewable energy instead of fossil fuels. Hydrogen (H_2) can be converted to electricity by using a fuel cell and such conversion generates only water as a by-product. Therefore, the establishment of a system in which H_2 is generated from water and solar energy by using a photocatalyst[1] is desirable, with the generated H_2 used for the generation of electricity from fuel cells (Scheme S1). Once such an energy-conversion system is established, it will be possible to circulate an energy medium (H_2) in addition to obtaining electricity only from solar energy and abundant water resources. However, realization of such an ultimate energy-conversion system requires further improvement of the reaction efficiency of water splitting as well as fuel cells.

In many cases, the surface of water-splitting photocatalysts is coated with metal or metal oxide nanoparticles.[2–22] The loaded nanoparticles, called cocatalysts, promote charge separation and act as active sites in the water-splitting reaction (Scheme 1). Effective strategies to realize highly active photocatalysts include improvement of the semiconductor photocatalyst and the cocatalyst. The activity of the cocatalysts can be enhanced by decreasing the particle diameter and improving the dispersibility.[2–22] Previous studies have shown that the particle size of cocatalysts can be readily controlled in the small particle region when presynthesized nanoparticles/clusters are used as precursors.[26–30] In addition, previous studies have demonstrated that protection of the cocatalyst with a chromium oxide (Cr_2O_3) film prevents the photoreduction reaction of oxygen (O_2)

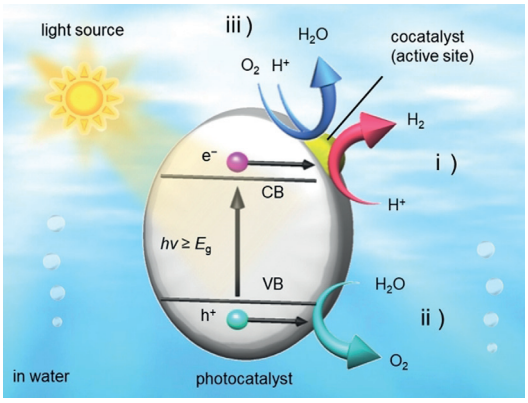

Scheme 1. Schematic of photocatalytic water splitting using a one-step photoexcitation system (CB, conduction band; VB, valence band; E_g, band gap) showing the processes of i) hydrogen evolution, ii) oxygen evolution, and iii) oxygen photoreduction.

[*] Dr. W. Kurashige, Y. Mori, S. Ozaki, M. Kawachi, Dr. S. Hossain, Dr. T. Kawawaki, Prof. A. Iwase, Prof. A. Kudo, Prof. Y. Negishi
Department of Applied Chemistry, Faculty of Science
Tokyo University of Science
1–3 Kagurazaka, Shinjuku-ku, Tokyo 162-8601 (Japan)
E-mail: negishi@rs.kagu.tus.ac.jp
Dr. T. Kawawaki, Prof. A. Iwase, Prof. A. Kudo, Prof. Y. Negishi
Research Institute for Science & Technology, Tokyo University of Science
1–3 Kagurazaka, Shinjuku-ku, Tokyo 162-8601 (Japan)
Dr. C. J. Shearer, Prof. G. F. Metha
Department of Chemistry, University of Adelaide
Adelaide, South Australia 5005 (Australia)
Prof. S. Yamazoe
Department of Chemistry, Graduate School of Science, Tokyo Metropolitan University
1-1 Minami-Osawa, Hachioji-shi, Tokyo 192-0397 (Japan)
Supporting information and the ORCID identification number(s) for the author(s) of this article can be found under: https://doi.org/10.1002/anie.201916681.

(Scheme 1), which is one of the back reactions of water splitting.[31–41] We previously prepared a water-splitting photocatalyst with relatively high activity by applying both of the aforementioned techniques to a gold (Au) cocatalyst-supported $BaLa_4Ti_4O_{15}$ photocatalyst (Figure S1).[42,43]

However, a volcano plot of H_2 adsorption and desorption[44] predicted that rhodium (Rh) should show higher activity than Au as a cocatalyst for H_2 production. Therefore, it is expected that loading an ultrafine cocatalyst composed of Rh and Cr oxides onto a photocatalyst surface will lead to higher water-splitting activity. Actually, Maeda and co-workers[45–48] reported that a photocatalyst loaded with Rh^{III}–Cr^{III} mixed oxide nanoparticles ($Rh_{2-x}Cr_xO_3$, 10–30 nm) showed higher water-splitting activity than a photocatalyst loaded with other nanoparticles. The activity of the photocatalyst seemed to increase with the use of finer $Rh_{2-x}Cr_xO_3$ nanoparticles. However, it is very difficult to load ultrafine (< 2 nm) particles onto photocatalysts by using common methods, such as impregnation or photodeposition.[45–48] In addition, it is also difficult to load the small $Rh_{2-x}Cr_xO_3$ particles onto the photocatalysts by using the loading method developed in the previous studies[42,43] because there are no precise synthesis method for small $Rh_{2-x}Cr_xO_3$ clusters, which is different from the case with Au clusters.

In this study, we attempted to load small $Rh_{2-x}Cr_xO_3$ cluster cocatalysts, by using the aggregation of a Rh–thiolate complex, onto the surface of the photocatalysts. As a result, we have succeeded in loading $Rh_{2-x}Cr_xO_3$ particles with a size of approximately 1.3 nm and a narrow size distribution onto a $BaLa_4Ti_4O_{15}$ photocatalyst ($Rh_{2-x}Cr_xO_3$(1.3 nm)/$BaLa_4Ti_4O_{15}$). Scanning transmission electron microscopy coupled with energy-dispersive X-ray spectroscopy (STEM-EDX) and X-ray absorption fine structure (XAFS) measurements revealed that the loaded particles were an oxide solid solution composed of Rh^{III} and Cr^{III} species. Moreover, $Rh_{2-x}Cr_xO_3$(1.3 nm)/$BaLa_4Ti_4O_{15}$ showed higher water-splitting activity than that of previously reported $BaLa_4Ti_4O_{15}$ loaded with fine ($\approx$1.2 nm) Au-cocatalyst nanoparticles protected by a Cr_2O_3 film[42,43] and $BaLa_4Ti_4O_{15}$ loaded with $\approx$3 nm $Rh_{2-x}Cr_xO_3$ particles ($Rh_{2-x}Cr_xO_3$(3.0 nm)/$BaLa_4Ti_4O_{15}$) prepared via the impregnation method.

Results and Discussion

$BaLa_4Ti_4O_{15}$ (Figure S1), which is a most advanced photocatalyst, was used in this work. $Rh_{2-x}Cr_xO_3$ particles ($\approx$1.3 nm) were loaded onto the $BaLa_4Ti_4O_{15}$ surface by the method summarized in Figure 1. Firstly, a Cr_2O_3 layer was formed on $BaLa_4Ti_4O_{15}$ (Figure 1a) by photodeposition to form Cr_2O_3/$BaLa_4Ti_4O_{15}$ (Figure 1b).[42,43] Then, a Rh–glutathionate (SG, Figure S2) complex with a molecular size slightly under 1 nm was adsorbed on the surface of Cr_2O_3/$BaLa_4Ti_4O_{15}$ to give Rh–SG/Cr_2O_3/$BaLa_4Ti_4O_{15}$ (Figure 1c). Next, Rh–SG/Cr_2O_3/$BaLa_4Ti_4O_{15}$ was calcined at 300 °C under reduced pressure to remove the ligands from the Rh–SG complex and form a solid solution of Rh and Cr oxides ($Rh_{2-x}Cr_xO_y$/$BaLa_4Ti_4O_{15}$, Figure 1d). Finally, a small amount of Cr with a high oxidation state ($y > 3$) was reduced to Cr^{III} by using ultraviolet (UV) light irradiation ($Rh_{2-x}Cr_xO_3$-(1.3 nm)/$BaLa_4Ti_4O_{15}$, Figure 1e).[42,43]

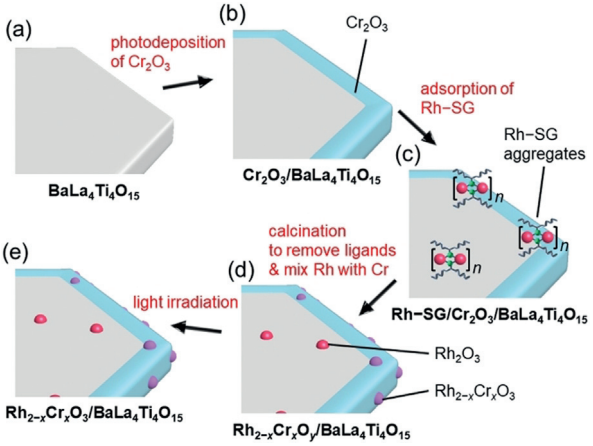

Figure 1. Schematic of the experimental procedure. (a) $BaLa_4Ti_4O_{15}$, (b) $Cr_2O_3/BaLa_4Ti_4O_{15}$, (c) Rh–SG/$Cr_2O_3/BaLa_4Ti_4O_{15}$, (d) $Rh_{2-x}Cr_xO_y$/$BaLa_4Ti_4O_{15}$, and (e) $Rh_{2-x}Cr_xO_3/BaLa_4Ti_4O_{15}$. $Rh_{2-x}Cr_xO_y$ indicates $Rh_{2-x}Cr_xO_3$ including highly oxidized Cr (> 3+).

The high-resolution (HR)-TEM images of the Cr_2O_3/$BaLa_4Ti_4O_{15}$ is shown in Figure 2. The Cr_2O_3 layers were mainly observed at the edge of $BaLa_4Ti_4O_{15}$ (Figure S3–S5). The reduction of the metal ions occurs more easily at the edge of $BaLa_4Ti_4O_{15}$ than at the flat surface of $BaLa_4Ti_4O_{15}$,[49] therefore, the Cr_2O_3 layers seem to be formed preferentially at the edge of $BaLa_4Ti_4O_{15}$ (Figure 1a).

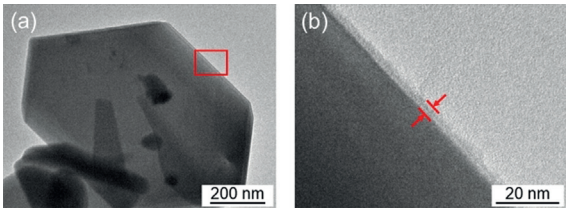

Figure 2. HR-TEM images of $Cr_2O_3/BaLa_4Ti_4O_{15}$ observed at (a) low and (b) high magnification for the edge of $BaLa_4Ti_4O_{15}$ (Figure S3 and S4). The image (b) is an expansion of the red square in image (a). In this experiment, Cr was loaded at 1 wt% to easily monitor the position of the Cr_2O_3 layers. For the HR-TEM image of $Cr_2O_3/BaLa_4Ti_4O_{15}$ with 0.1 wt%, see Figure S5.

The Rh–SG complex was prepared by mixing $RhCl_3$ with glutathione (GSH, Figure S2) in water, followed by the addition of a reducing agent. The optical absorption spectrum of the product is shown in Figure 3a. A peak attributed to charge transfer from SG to Rh (ligand-to-metal charge transfer; LMCT)[50] was observed near 350 nm, indicating the formation of the Rh–S bond. This bond formation was also confirmed by Fourier transform (FT) infrared (IR) absorption[51] (Figure 3b and S6) and Rh K-edge FT extended X-ray absorption fine structure (EXAFS) spectroscopies[52] (Figure 3c). The electrospray ionization (ESI) mass spectrum of the product (Figure S7) is shown in Figure 3d. This spectrum revealed that the Rh–SG complex mainly contained

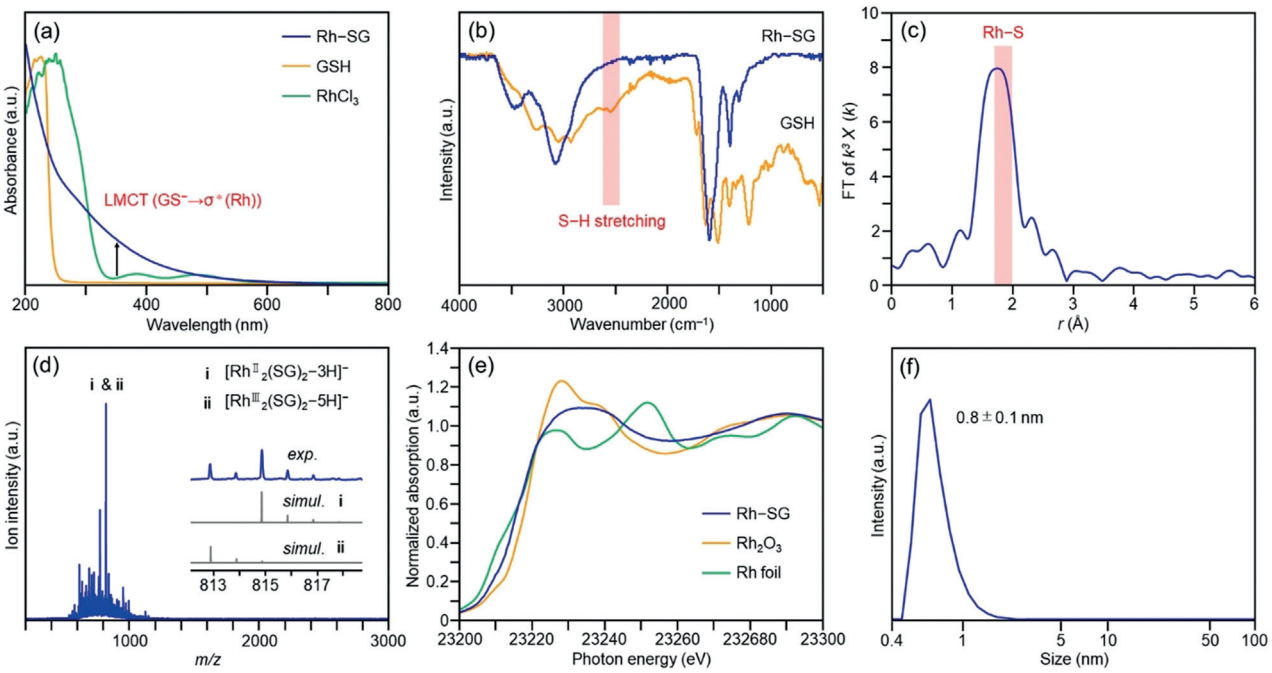

Figure 3. Characterization of the Rh–SG complex. (a) Comparison of the optical absorption spectra of Rh–SG, $RhCl_3$, and GSH. (b) Comparison of FT-IR spectra of Rh–SG and GSH (Figure S6). (c) Rh K-edge FT-EXAFS of Rh–SG. (d) Negative-ion ESI mass spectrum of Rh–SG (Figure S7), showing that the main products are $Rh_2(SG)_2$ containing Rh^{II} (i) or Rh^{III} (ii) (Table S1). (e) Comparison of K-edge XANES spectra of Rh–SG, Rh_2O_3, and Rh foil, confirming that Rh in Rh–SG is oxidized. (f) DLS spectrum of Rh–SG, showing that the Rh–SG complex has an average diameter of 0.8 nm in water.

Rh^{II} and Rh^{III} species (Figure 3d and Table S1). A similar interpretation was also obtained from the Rh K-edge X-ray absorption near-edge structure (XANES) spectrum (Figure 3e); the XANES spectrum is not consistent with that of Rh^{III} because of a distribution in the charge state of Rh in Rh–SG complex. A dynamic light scattering (DLS) measurement revealed that the obtained Rh–SG complex had a molecular size of around 0.8 nm in solution (Figure 3f).

The Rh–SG complex was adsorbed onto Cr_2O_3/$BaLa_4Ti_4O_{15}$ by stirring the materials together in water (Figure 1c). Inductively coupled plasma mass spectrometry (ICP-MS) analysis of the supernatant confirmed that the Rh–SG complex was adsorbed onto the photocatalyst surface with a relatively high adsorption rate (Table S2). In water, the surface of Cr_2O_3 is in the state of $CrO_{(1.5-m)}(OH)_{2m}{\cdot}xH_2O$ ($m = 0$, 0.5, or 1.5).[53] Moreover, the bare surface of $BaLa_4Ti_4O_{15}$ lacking Cr_2O_3 has also hydroxyl groups (-OH).[54] It is considered that because the polar functional groups in the ligand of the Rh–SG complex, such as carboxyl and amino groups (Figure S2), formed hydrogen bonds with the -OH groups on the photocatalyst surface, the Rh–SG complex was adsorbed on Cr_2O_3/$BaLa_4Ti_4O_{15}$ at a high adsorption rate (Figure S8 and S9).

Rh–SG/Cr_2O_3/$BaLa_4Ti_4O_{15}$ was calcined at 300 °C (Figure S10 and S11) under reduced pressure ($> 1.0 \times 10^{-1}$ Pa; Figure 1d). The S 2p photoelectron spectra before and after calcination of the $BaLa_4Ti_4O_{15}$ photocatalyst containing 0.09 wt% Rh and 0.10 wt% Cr are shown in Figure 4Aa and 4Ab. Before calcination (Rh–SG/Cr_2O_3/$BaLa_4Ti_4O_{15}$), a peak attributed to S $2p_{3/2}$ was observed near 161.2 eV (Figure 4Aa).[55] After calcination ($Rh_{2-x}Cr_xO_y$/$BaLa_4Ti_4O_{15}$), this peak disappeared (Figure 4Ab), implying that SG was removed by calcination.[42,43] The elemental mapping of this photocatalyst before and after calcination is depicted in Figure 4Ba and 4Bb, respectively, obtained by STEM-EDX. Before calcination (Rh–SG/Cr_2O_3/$BaLa_4Ti_4O_{15}$), Rh was present on the Cr_2O_3 film (Figure 4Ba). After calcination ($Rh_{2-x}Cr_xO_y$/$BaLa_4Ti_4O_{15}$), both Rh and Cr were found in the same layer (Figure 4Bb). This phenomenon was also confirmed from the line analysis of the elemental mapping (Figure 4C). These results indicate that Rh and Cr species mixed during calcination (Figure 5). The Rh K-edge XANES spectra of the photocatalyst before and after irradiation is shown in Figure 6A. The Rh K-edge XANES spectrum of the calcined sample ($Rh_{2-x}Cr_xO_y$/$BaLa_4Ti_4O_{15}$) greatly differs from that of Rh foil, but it resembles that of $Rh_{1.5}Cr_{0.5}O_3$.[45–48] The estimated number of Rh−O bonds in the sample after calcination (Figure S12) is similar to that in Rh_2O_3 and $Rh_{1.5}Cr_{0.5}O_3$ (Table S3). The Cr K-edge XANES spectra of the sample before and after irradiation is depicted in Figure 6B. After calcination ($Rh_{2-x}Cr_xO_y$/$BaLa_4Ti_4O_{15}$), the intensity of the Cr K-edge XANES spectrum at an absorption edge near 6010 eV is stronger than that of Cr foil. This indicates that the Cr in the sample after calcination ($Rh_{2-x}Cr_xO_y$/$BaLa_4Ti_4O_{15}$) was oxidized.[56] In the TEM image of $Rh_{2-x}Cr_xO_y$/$BaLa_4Ti_4O_{15}$ (Figure 6Ca), very fine particles (1.2 ± 0.2 nm) were observed. These results indicate that calcination resulted in the loading of ultrafine Rh^{III}–(Cr^{III}, Cr^{VI}) mixed oxide particles onto the $BaLa_4Ti_4O_{15}$ surface. It is considered that because Rh and Cr tend to form mixed oxides when

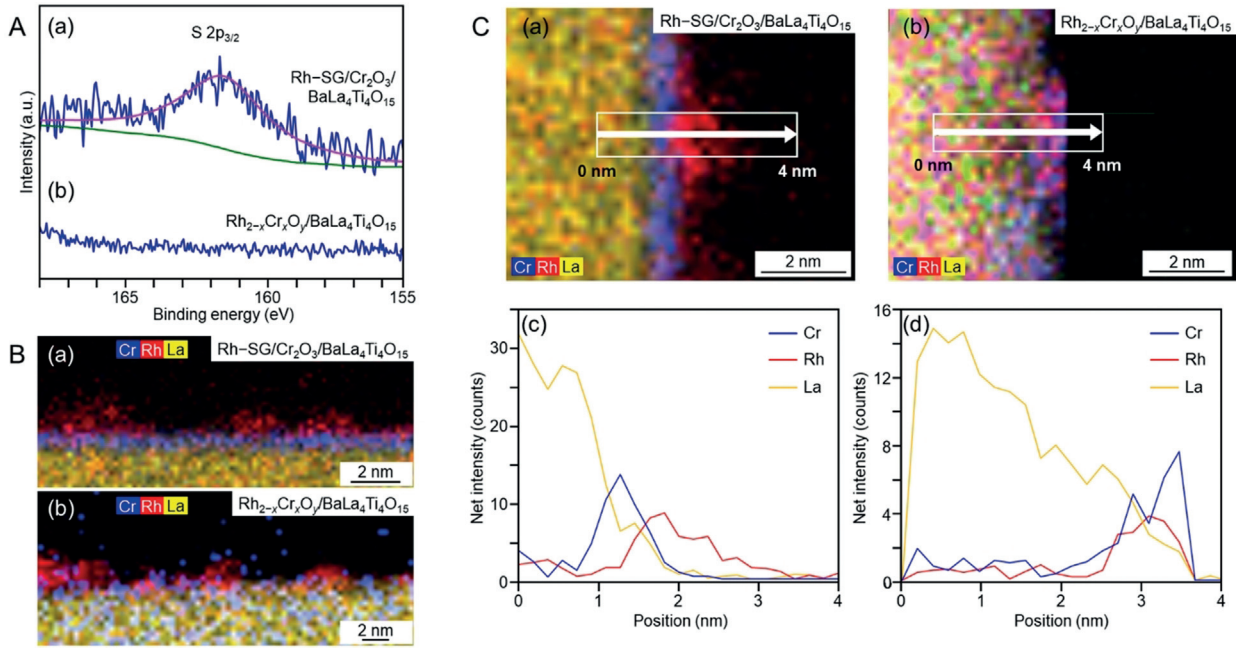

Figure 4. Characterization of the $BaLa_4Ti_4O_{15}$ photocatalyst containing 0.09 wt% Rh and 0.10 wt% Cr. (A) S 2p photoelectron spectra and (B) STEM-EDX elemental mapping for (a) Rh–SG/Cr_2O_3/$BaLa_4Ti_4O_{15}$ and (b) $Rh_{2-x}Cr_xO_y$/$BaLa_4Ti_4O_{15}$. (C) Line analysis of elemental mapping for (a),(c) Rh–SG/Cr_2O_3/$BaLa_4Ti_4O_{15}$ and (b),(d) $Rh_{2-x}Cr_xO_y$/$BaLa_4Ti_4O_{15}$.

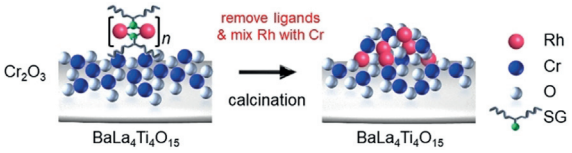

Figure 5. Schematic of the phenomenon that occurred during calcination process (Figure 4 B,C).

heated,[45,46] the calcination process induced the formation of mixed oxide particles as well as SG ligand removal (Figure 5).

Immediately after calcination (Figure 1 d), part of the Cr species in the sample was oxidized to a higher oxidation state than Cr^{III}.[42,43] Then, the obtained photocatalyst was irradiated with UV light for 1 h to reduce the Cr species in the higher oxidation state to Cr^{III} (Figure 1 e).[42,43] The Cr K-edge XANES spectrum confirmed that the Cr species in the higher oxidation state was reduced by the UV light irradiation (Figure 6 B and S13). This process had little effect on the oxidation state of the Rh species (Figure 6 A). Moreover, during the series of reaction steps in Figure 1, the crystalline structure of $BaLa_4Ti_4O_{15}$ barely changed (Figure S14). In the TEM image of the obtained $Rh_{2-x}Cr_xO_3$/$BaLa_4Ti_4O_{15}$ (Figure 6 Cb), particles with a size of 1.3 ± 0.3 nm were observed. These results demonstrate that the developed loading method enabled very fine $Rh_{2-x}Cr_xO_3$ particles (≈ 1.3 nm) with a narrow size distribution to be loaded onto the $BaLa_4Ti_4O_{15}$ surface ($Rh_{2-x}Cr_xO_3$(1.3 nm)/$BaLa_4Ti_4O_{15}$).

Considering the particle size of $Rh_{2-x}Cr_xO_3$ of 1.3 ± 0.3 nm, the obtained $Rh_{2-x}Cr_xO_3$ particles should be formed from several Rh–SG complexes. Particles of this size were probably formed (Figure S15) because several Rh–SG complexes aggregated onto $BaLa_4Ti_4O_{15}$ during the adsorption process (Figure 4 Ba, 4 Ca, and Figure 5). The size of the loaded $Rh_{2-x}Cr_xO_3$ particles did not change when the loading amount of Rh was altered in the range of 0.05 to 0.13 wt% (Figure S16). This finding means that such a small difference of the concentration of Rh–SG complexes in solution hardly affected the degree of aggregation of Rh–SG complexes onto the $BaLa_4Ti_4O_{15}$ surface during the adsorption process.

The water-splitting activity of the obtained $Rh_{2-x}Cr_xO_3$-(1.3 nm)/$BaLa_4Ti_4O_{15}$ photocatalyst was then examined. Specifically, $Rh_{2-x}Cr_xO_3$(1.3 nm)/$BaLa_4Ti_4O_{15}$ (500 mg) was dispersed in water and irradiated with UV light from a high-pressure mercury (Hg) lamp (Figure S17).[42,43] Water-splitting experiments using a series of samples (Figure S16 b) revealed that $Rh_{2-x}Cr_xO_3$(1.3 nm)/$BaLa_4Ti_4O_{15}$ containing 0.09 wt% Rh and 0.10 wt% Cr exhibited the highest activity (Figure S18). For this photocatalyst, almost no decrease in activity (Figure 7) and no increase in particle size (Figure 8) were observed even after 10 h of water-splitting reaction. Moreover, it was confirmed that the reverse reaction (Figure S19 a and S20) and the O_2 photoreduction reaction (Figure S19 b and S21) were well suppressed over this sample, as expected.

The gas-evolution rate of $Rh_{2-x}Cr_xO_3$(1.3 nm)/$BaLa_4Ti_4O_{15}$ containing 0.09 wt% Rh and 0.10 wt% Cr (Table 1) is shown in Figure 9 a; this photocatalyst exhibited the highest activity of the investigated photocatalysts (Figure S18). The ratio of the generated H_2 and O_2 amount was close to 2:1, indicating that the water-splitting reaction proceeded ideally. The water-splitting activity of this sample was approximately four times higher than that of $BaLa_4Ti_4O_{15}$ loaded with Au_{25} clusters[57–67] protected by a Cr_2O_3 film (Au_{25}@Cr_2O_3/$BaLa_4Ti_4O_{15}$)[42,43] (Figure 9 b and Table 1). Moreover, the $Rh_{2-x}Cr_xO_3$(1.3 nm)/$BaLa_4Ti_4O_{15}$ photocatalyst also showed

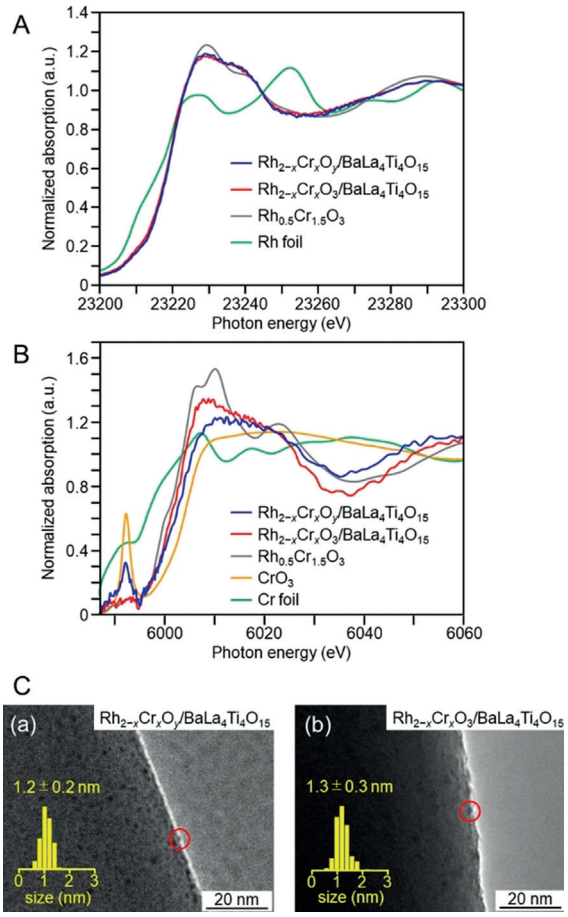

Figure 6. Characterization of the $BaLa_4Ti_4O_{15}$ photocatalyst containing 0.09 wt% Rh and 0.10 wt% Cr. (A) Rh K-edge XANES spectra of $Rh_{2-x}Cr_xO_y/BaLa_4Ti_4O_{15}$ and $Rh_{2-x}Cr_xO_3/BaLa_4Ti_4O_{15}$ together with those of Rh foil and $Rh_{0.5}Cr_{1.5}O_3$. (B) Cr K-edge XANES spectra of $Rh_{2-x}Cr_xO_y/BaLa_4Ti_4O_{15}$ and $Rh_{2-x}Cr_xO_3/BaLa_4Ti_4O_{15}$ together with those of Cr foil, CrO_3, and $Rh_{0.5}Cr_{1.5}O_3$. (C) TEM images of (a) $Rh_{2-x}Cr_xO_y/BaLa_4Ti_4O_{15}$ and (b) $Rh_{2-x}Cr_xO_3/BaLa_4Ti_4O_{15}$. In (C), the red circles indicate the $Rh_{2-x}Cr_xO_y$ or $Rh_{2-x}Cr_xO_3$ particles.

higher water-splitting activity than that of $BaLa_4Ti_4O_{15}$ loaded with 0.50 wt% Ni ($Ni_{NP}@NiO_x/BaLa_4Ti_4O_{15}$, Figure S22), which exhibited the highest water-splitting activity of previously reported $BaLa_4Ti_4O_{15}$ catalysts (Figure 9c and Table 1).[49] These results demonstrate that the use of $Rh_{2-x}Cr_xO_3$ particles as a cocatalyst is also very effective for improving the water-splitting activity of $BaLa_4Ti_4O_{15}$.[45–48,68,69] $Rh_{2-x}Cr_xO_3$(1.3 nm)/$BaLa_4Ti_4O_{15}$ containing 0.09 wt% Rh and 0.10 wt% Cr showed an apparent quantum yield of 16% under 270 nm excitation.

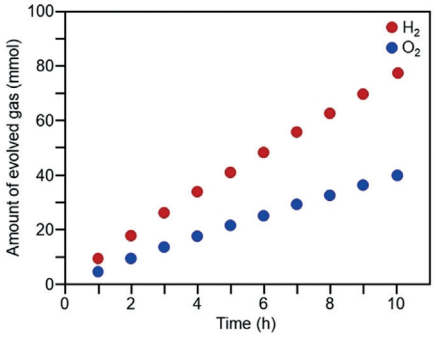

Figure 7. Time course of water splitting over $Rh_{2-x}Cr_xO_3$(1.3 nm)/$BaLa_4Ti_4O_{15}$ with 0.09 wt% Rh and 0.10 wt% Cr. The activity hardly decreased during 10 h of the water-splitting reaction.

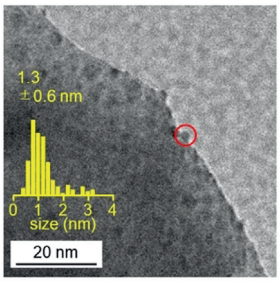

Figure 8. TEM image of $Rh_{2-x}Cr_xO_3$(1.3 nm)/$BaLa_4Ti_4O_{15}$ containing 0.09 wt% Rh and 0.10 wt% Cr after 10 h of the water-splitting reaction. The average size of $Rh_{2-x}Cr_xO_3$ particles after 10 h of the reaction was similar to that before the reaction (Figure 6C(b)).

To examine the importance of the preparation method used in this study, we also attempted to load the $Rh_{2-x}Cr_xO_3$ particles onto $BaLa_4Ti_4O_{15}$ by impregnation (Figure S23) and photodeposition methods (Figure S24). We found that these techniques could not form $Rh_{2-x}Cr_xO_3$ particles with a size comparable to that achieved by the method developed in this study. Therefore, our technique is important because it allows loading of ultrafine $Rh_{2-x}Cr_xO_3$ particles. The impregnation method allowed loading of $Rh_{2-x}Cr_xO_3$ particles onto $BaLa_4Ti_4O_{15}$ to give a photocatalyst with 0.10 wt% Rh and 0.15 wt% Cr with a particle size of 3.0 ± 2.3 nm ($Rh_{2-x}Cr_xO_3$(3.0 nm)/$BaLa_4Ti_4O_{15}$; Figure S23). This photocatalyst showed the highest water-splitting activity among the $Rh_{2-x}Cr_xO_3/BaLa_4Ti_4O_{15}$ photocatalysts prepared by the impregnation and photodeposition methods (Figure S24). However, the gas-evolution rate of $Rh_{2-x}Cr_xO_3$(3.0 nm)/$BaLa_4Ti_4O_{15}$ was ≈74% of that of $Rh_{2-x}Cr_xO_3$(1.3 nm)/$BaLa_4Ti_4O_{15}$ prepared by our technique (Figure 9d and Table 1).

Table 1: Gas-evolution rates over various photocatalysts.

Photocatalyst	Ratio of cocatalysts elements	Loading of cocatalysts	H_2 [mmol h^{-1}]	O_2 [mmol h^{-1}]
$Rh_{2-x}Cr_xO_3$(1.3 nm)/$BaLa_4Ti_4O_{15}$	0.09 wt% Rh and 0.10 wt% Cr	this method[a]	9.9	5.1
$Au_{25}@Cr_2O_3/BaLa_4Ti_4O_{15}$	0.10 wt% Au and 0.50 wt% Cr	our previous method[b]	2.4	1.2
$Ni_{NP}@NiO_x/BaLa_4Ti_4O_{15}$	0.50 wt% Ni	impregnation	1.2	0.6
$Rh_{2-x}Cr_xO_3$(3.0 nm)/$BaLa_4Ti_4O_{15}$	0.10 wt% Rh and 0.15 wt% Cr	impregnation	7.3	3.6

[a] Photodeposition of Cr_2O_3 + adsorption of Rh–SG complexes + calcination of photocatalysts. [b] Photodeposition of Cr_2O_3 + adsorption of SG-protected Au_{25} cluster + calcination of photocatalysts.[43]

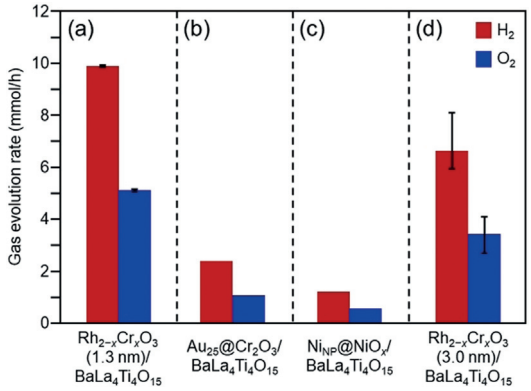

Figure 9. Comparison of gas-evolution rates over different photocatalysts (a) $Rh_{2-x}Cr_xO_3$(1.3 nm)/$BaLa_4Ti_4O_{15}$ (0.09 wt% Rh and 0.10 wt% Cr), (b) $Au_{25}@Cr_2O_3/BaLa_4Ti_4O_{15}$ (0.10 wt% Au and 0.50 wt% Cr), (c) $Ni_{NP}@NiO_x/BaLa_4Ti_4O_{15}$ (0.50 wt% Ni),[67] and (d) $Rh_{2-x}Cr_xO_3$-(3.0 nm)/$BaLa_4Ti_4O_{15}$ (0.10 wt% Rh and 0.15 wt% Cr) (Table 1).

These two photocatalysts were prepared via different methods, therefore, there may be additional differences other than the size of the $Rh_{2-x}Cr_xO_3$ particles, such as the position of cocatalysts on the surface, that contribute to the higher water-splitting activity of $Rh_{2-x}Cr_xO_3$(1.3 nm)/$BaLa_4Ti_4O_{15}$ compared with that of $Rh_{2-x}Cr_xO_3$(3.0 nm)/$BaLa_4Ti_4O_{15}$ (Figure S25). Overall, this study demonstrates that loading ultrafine $Rh_{2-x}Cr_xO_3$ particles by the developed technique is an effective approach to improve the water-splitting activity of $BaLa_4Ti_4O_{15}$.

Conclusion

We loaded ultrafine $Rh_{2-x}Cr_xO_3$ particles with a size of approximately 1.3 nm and a narrow size distribution onto the $BaLa_4Ti_4O_{15}$ photocatalyst by establishing a new loading method for the $Rh_{2-x}Cr_xO_3$ particles. The obtained photocatalyst exhibited a remarkably high quantum yield for water splitting compared to that achieved for $BaLa_4Ti_4O_{15}$ in previous studies. Although this study used only $BaLa_4Ti_4O_{15}$ as the photocatalyst,[42,43] the developed loading method can, in principal, be applied to other photocatalysts as well. $Rh_{2-x}Cr_xO_3$ particles are a useful cocatalyst for many water-splitting photocatalysts,[45–48,68,69] therefore, we expect that this loading method should also be suitable to improve the water-splitting activity of other advanced photocatalysts.

Acknowledgements

This work was supported by the Japan Society for the Promotion of Science (JSPS) KAKENHI, Scientific Research on Innovative Areas "Coordination Asymmetry" (grant number 17H05385), and Scientific Research on Innovative Areas "Innovations for Light-Energy Conversion" (grant number 18H05178). The authors acknowledge the STEM facilities and scientific and technical assistance of Dr. Ashley Slattery at Adelaide Microscopy (University of Adelaide), part of Microscopy Australia.

Conflict of interest

The authors declare no conflict of interest.

Keywords: cocatalysts · metal clusters · nanostructures · photocatalysts · water splitting

How to cite: *Angew. Chem. Int. Ed.* **2020**, *59*, 7076–7082
Angew. Chem. **2020**, *132*, 7142–7148

[1] A. Fujishima, K. Honda, *Nature* **1972**, *238*, 37–38.
[2] A. Yamakata, T. Ishibashi, H. Kato, A. Kudo, H. Onishi, *J. Phys. Chem. B* **2003**, *107*, 14383–14387.
[3] T. Hisatomi, J. Kubota, K. Domen, *Chem. Soc. Rev.* **2014**, *43*, 7520–7535.
[4] J. Sato, N. Saito, Y. Yamada, K. Maeda, T. Takata, J. N. Kondo, M. Hara, H. Kobayashi, K. Domen, Y. Inoue, *J. Am. Chem. Soc.* **2005**, *127*, 4150–4151.
[5] J. Yang, D. Wang, H. Han, C. Li, *Acc. Chem. Res.* **2013**, *46*, 1900–1909.
[6] K. Maeda, K. Teramura, D. Lu, T. Takata, N. Saito, Y. Inoue, K. Domen, *Nature* **2006**, *440*, 295.
[7] A. Kudo, Y. Miseki, *Chem. Soc. Rev.* **2009**, *38*, 253–278.
[8] M. Yoshida, K. Maeda, D. Lu, J. Kubota, K. Domen, *J. Phys. Chem. C* **2013**, *117*, 14000–14006.
[9] Q. Li, B. Guo, J. Yu, J. Ran, B. Zhang, H. Yan, J. R. Gong, *J. Am. Chem. Soc.* **2011**, *133*, 10878–10884.
[10] Z. Zou, J. Ye, K. Sayama, H. Arakawa, *Nature* **2001**, *414*, 625–627.
[11] Q. Wang, T. Hisatomi, Q. Jia, H. Tokudome, M. Zhong, C. Wang, Z. Pan, T. Takata, M. Nakabayashi, N. Shibata, Y. Li, I. D. Sharp, A. Kudo, T. Yamada, K. Domen, *Nat. Mater.* **2016**, *15*, 611–615.
[12] Q. Xiang, J. Yu, M. Jaroniec, *J. Am. Chem. Soc.* **2012**, *134*, 6575–6578.
[13] R. Abe, M. Higashi, K. Domen, *J. Am. Chem. Soc.* **2010**, *132*, 11828–11829.
[14] F. E. Osterloh, *Chem. Mater.* **2008**, *20*, 35–54.
[15] S. U. M. Khan, M. Al-Shahry, W. B. Ingler, Jr., *Science* **2002**, *297*, 2243–2245.
[16] X. Chen, S. Shen, L. Guo, S. S. Mao, *Chem. Rev.* **2010**, *110*, 6503–6570.
[17] X. Wang, K. Maeda, A. Thomas, K. Takanabe, G. Xin, J. M. Carlsson, K. Domen, M. Antonietti, *Nat. Mater.* **2009**, *8*, 76–80.
[18] Y. Wang, H. Suzuki, J. Xie, O. Tomita, D. J. Martin, M. Higashi, D. Kong, R. Abe, J. Tang, *Chem. Rev.* **2018**, *118*, 5201–5241.
[19] D. M. Fabian, S. Hu, N. Singh, F. A. Houle, T. Hisatomi, K. Domen, F. E. Osterloh, S. Ardo, *Energy Environ. Sci.* **2015**, *8*, 2825–2850.
[20] H. G. Kim, D. W. Hwang, J. S. Lee, *J. Am. Chem. Soc.* **2004**, *126*, 8912–8913.
[21] A. Mukherji, B. Seger, G. Q. M. Lu, L. Wang, *ACS Nano* **2011**, *5*, 3483–3492.
[22] K. Maeda, *ACS Catal.* **2013**, *3*, 1486–1503.
[23] M. Hara, J. T. Lean, T. E. Mallouk, *Chem. Mater.* **2001**, *13*, 4668–4675.
[24] J. Liu, Y. Liu, N. Liu, Y. Han, X. Zhang, H. Huang, Y. Lifshitz, S.-T. Lee, J. Zhong, Z. Kang, *Science* **2015**, *347*, 970–974.
[25] S. Linic, P. Christopher, D. B. Ingram, *Nat. Mater.* **2011**, *10*, 911–921.

[26] T. Ikeda, A. Xiong, T. Yoshinaga, K. Maeda, K. Domen, T. Teranishi, *J. Phys. Chem. C* **2013**, *117*, 2467 – 2473.
[27] N. Sakamoto, H. Ohtsuka, T. Ikeda, K. Maeda, D. Lu, M. Kanehara, K. Teramura, T. Teranishi, K. Domen, *Nanoscale* **2009**, *1*, 106 – 109.
[28] Y. Negishi, Y. Matsuura, R. Tomizawa, W. Kurashige, Y. Niihori, T. Takayama, A. Iwase, A. Kudo, *J. Phys. Chem. C* **2015**, *119*, 11224 – 11232.
[29] F. Xue, C. Chen, W. Fu, M. Liu, C. Liu, P. Guo, S. Shen, *J. Phys. Chem. C* **2018**, *122*, 25165 – 25173.
[30] D. Wang, Z.-P. Liu, W.-M. Yang, *ACS Catal.* **2018**, *8*, 7270 – 7278.
[31] K. Maeda, K. Teramura, D. Lu, N. Saito, Y. Inoue, K. Domen, *Angew. Chem. Int. Ed.* **2006**, *45*, 7806 – 7809; *Angew. Chem.* **2006**, *118*, 7970 – 7973.
[32] M. Yoshida, K. Takanabe, K. Maeda, A. Ishikawa, J. Kubota, Y. Sakata, Y. Ikezawa, K. Domen, *J. Phys. Chem. C* **2009**, *113*, 10151 – 10157.
[33] Y.-J. Cho, G.-H. Moon, T. Kanazawa, K. Maeda, W. Choi, *Chem. Commun.* **2016**, *52*, 9636 – 9639.
[34] F. Dionigi, P. C. K. Vesborg, T. Pedersen, O. Hansen, S. Dahl, A. Xiong, K. Maeda, K. Domen, I. Chorkendorff, *J. Catal.* **2012**, *292*, 26 – 31.
[35] K. Maeda, N. Sakamoto, T. Ikeda, H. Ohtsuka, A. Xiong, D. Lu, M. Kanehara, T. Teranishi, K. Domen, *Chem. Eur. J.* **2010**, *16*, 7750 – 7759.
[36] K. Maeda, A. Xiong, T. Yoshinaga, T. Ikeda, N. Sakamoto, T. Hisatomi, M. Takashima, D. Lu, M. Kanehara, T. Setoyama, T. Teranishi, K. Domen, *Angew. Chem. Int. Ed.* **2010**, *49*, 4096 – 4099; *Angew. Chem.* **2010**, *122*, 4190 – 4193.
[37] K. E. Sanwald, T. F. Berto, A. Jentys, D. M. Camaioni, O. Y. Gutiérrez, J. A. Lercher, *ACS Catal.* **2018**, *8*, 2902 – 2913.
[38] K. Maeda, K. Teramura, D. Lu, N. Saito, Y. Inoue, K. Domen, *J. Phys. Chem. C* **2007**, *111*, 7554 – 7560.
[39] T. Takata, C. Pan, M. Nakabayashi, N. Shibata, K. Domen, *J. Am. Chem. Soc.* **2015**, *137*, 9627 – 9634.
[40] K. Maeda, D. Lu, K. Domen, *Chem. Eur. J.* **2013**, *19*, 4986 – 4991.
[41] P. Ravi, V. N. Rao, M. V. Shankar, M. Sathish, *Int. J. Hydrogen Energy* **2018**, *43*, 3976 – 3987.
[42] W. Kurashige, R. Hayashi, K. Wakamatsu, Y. Kataoka, S. Hossain, A. Iwase, A. Kudo, S. Yamazoe, Y. Negishi, *ACS Appl. Energy Mater.* **2019**, *2*, 4175 – 4187.
[43] W. Kurashige, R. Kumazawa, D. Ishii, R. Hayashi, Y. Niihori, S. Hossain, L. V. Nair, T. Takayama, A. Iwase, S. Yamazoe, T. Tsukuda, A. Kudo, Y. Negishi, *J. Phys. Chem. C* **2018**, *122*, 13669 – 13681.
[44] S. Trasatti, *J. Electroanal. Chem.* **1972**, *39*, 163 – 184.
[45] T. Hisatomi, K. Maeda, K. Takanabe, J. Kubota, K. Domen, *J. Phys. Chem. C* **2009**, *113*, 21458 – 21466.
[46] K. Maeda, K. Teramura, H. Masuda, T. Takata, N. Saito, Y. Inoue, K. Domen, *J. Phys. Chem. B* **2006**, *110*, 13107 – 13112.
[47] T. Ohno, L. Bai, T. Hisatomi, K. Maeda, K. Domen, *J. Am. Chem. Soc.* **2012**, *134*, 8254 – 8259.
[48] K. Maeda, D. Lu, K. Teramura, K. Domen, *Energy Environ. Sci.* **2010**, *3*, 471 – 478.
[49] Y. Miseki, H. Kato, A. Kudo, *Energy Environ. Sci.* **2009**, *2*, 306 – 314.
[50] A. E. Garcia, F. Jalilehvand, *J. Biol. Inorg. Chem.* **2018**, *23*, 231 – 239.
[51] A. Barth, *Prog. Biophys. Mol. Biol.* **2000**, *74*, 141 – 173.
[52] E. Parthé, D. Hohnke, F. Hulliger, *Acta Crystallogr.* **1967**, *23*, 832 – 840.
[53] C. Sunseri, S. Piazza, F. D. Quarto, *J. Electrochem. Soc.* **1990**, *137*, 2411 – 2417.
[54] H. P. Boehm, *Discuss. Faraday Soc.* **1971**, *52*, 264 – 275.
[55] K. Uvdal, P. Bodö, B. Liedberg, *J. Colloid Interface Sci.* **1992**, *149*, 162 – 173.
[56] M. L. Peterson, G. E. Brown, Jr., G. A. Parks, C. L. Stein, *Geochim. Cosmochim. Acta* **1997**, *61*, 3399 – 3412.
[57] M. Zhu, C. M. Aikens, F. J. Hollander, G. C. Schatz, R. Jin, *J. Am. Chem. Soc.* **2008**, *130*, 5883 – 5885.
[58] Y. Negishi, K. Nobusada, T. Tsukuda, *J. Am. Chem. Soc.* **2005**, *127*, 5261 – 5270.
[59] Y. Shichibu, Y. Negishi, T. Tsukuda, T. Teranishi, *J. Am. Chem. Soc.* **2005**, *127*, 13464 – 13465.
[60] E. S. Shibu, M. A. H. Muhammed, T. Tsukuda, T. Pradeep, *J. Phys. Chem. C* **2008**, *112*, 12168 – 12176.
[61] S. Wang, Y. Song, S. Jin, X. Liu, J. Zhang, Y. Pei, X. Meng, M. Chen, P. Li, M. Zhu, *J. Am. Chem. Soc.* **2015**, *137*, 4018 – 4021.
[62] C. Yao, Y.-J. Lin, J. Yuan, L. Liao, M. Zhu, L.-H. Weng, J. Yang, Z. Wu, *J. Am. Chem. Soc.* **2015**, *137*, 15350 – 15353.
[63] A. Dass, A. Stevenson, G. R. Dubay, J. B. Tracy, R. W. Murray, *J. Am. Chem. Soc.* **2008**, *130*, 5940 – 5946.
[64] T. Chen, V. Fung, Q. Yao, Z. Luo, D.-E. Jiang, J. Xie, *J. Am. Chem. Soc.* **2018**, *140*, 11370 – 11377.
[65] Z. Luo, V. Nachammai, B. Zhang, N. Yan, D. T. Leong, D.-E. Jiang, J. Xie, *J. Am. Chem. Soc.* **2014**, *136*, 10577 – 10580.
[66] K. Kawamura, D. Hikosou, A. Inui, K. Yamamoto, J. Yagi, S. Saita, H. Kawasaki, *J. Phys. Chem. C* **2019**, *123*, 26644 – 26652.
[67] D. M. Black, C. M. Crittenden, J. S. Brodbelt, R. L. Whetten, *J. Phys. Chem. Lett.* **2017**, *8*, 1283 – 1289.
[68] Y. Sakata, T. Hayashi, R. Yasunaga, N. Yanaga, H. Imamura, *Chem. Commun.* **2015**, *51*, 12935 – 12938.
[69] T. H. Chiang, H. Lyu, T. Hisatomi, Y. Goto, T. Takata, M. Katayama, T. Minegishi, K. Domen, *ACS Catal.* **2018**, *8*, 2782 – 2788.

Manuscript received: December 30, 2019
Accepted manuscript online: February 11, 2020
Version of record online: March 6, 2020

